



Cite this: *Nanoscale*, 2014, **6**, 12470

Received 1st July 2014,  
Accepted 23rd August 2014

DOI: 10.1039/c4nr03672g

www.rsc.org/nanoscale

## Laser rapid thermal annealing enables tunable plasmonics in nanoporous gold nanoparticles†

Md Masud Parvez Arnob,<sup>a</sup> Fusheng Zhao,<sup>a</sup> Jianbo Zeng,<sup>a</sup> Gregg M. Santos,<sup>a</sup> Ming Li<sup>a</sup> and Wei-Chuan Shih<sup>\*a,b</sup>

A novel laser rapid thermal annealing (LRTA) technique is reported to tune the plasmonic resonance of disk-shaped nanoporous gold (NPG) nanoparticles for the first time. LRTA alters both the external and internal geometrical parameters of NPG nanoparticles at temperatures significantly lower than the melting temperature of bulk gold or non-porous gold nanoparticles. With increasing annealing laser intensity, the average pore size increases, while the mean disk diameter decreases. These morphological changes lead to blueshifting of the localized surface plasmon resonance (LSPR), which subsequently fine-tunes the SERS performance by better aligning the excitation laser and Raman scattering wavelengths with the LSPR peak. This technique can provide an effective means to optimize NPG nanoparticles for various plasmonic applications such as photothermal conversion, light-gated molecular release, and molecular sensing.

### Introduction

Light-excited collective oscillation of conduction band electrons, known as surface plasmon, has made metallic nanomaterials a recent research focus. In particular, nanoporous gold (NPG), a bi-continuous thin film of gold ligaments and void pores, has attracted much attention in the field of catalysis,<sup>1</sup> sensors,<sup>2</sup> actuators,<sup>3</sup> plasmonics,<sup>4</sup> and energy storage<sup>5</sup> due to its attractive properties such as large surface area,<sup>6</sup> chemical inertness,<sup>2</sup> biological compatibility,<sup>7</sup> etc. However, a semi-infinite NPG thin film exhibits weak plasmonic extinction and little plasmon resonance tunability due to its pore size being much smaller than the light wavelength.<sup>8</sup> Recently, our group has demonstrated that these limitations can be overcome by disk-shaped NPG nanoparticles with sub-wavelength diameter and sub-100 nm thickness.<sup>8</sup> Besides stronger plasmo-

nic extinction and wider plasmon resonance tuning, disk-shaped NPG nanoparticles, a.k.a. NPG disks, possess a large specific surface area and high-density internal plasmonic “hot-spots” with impressive electric field enhancement, which make them excellent nanoparticles to be employed in sensing, imaging, and photothermal applications.<sup>9–11</sup>

Since plasmonic properties of NPG nanoparticles play a significant role in potential applications, a technique to fine-tune its plasmonic resonance can be highly valuable. NPG nanoparticle plasmonics is controlled by its structural and morphological features which can be classified into two different (internal and external) regimes. The internal regime refers to the nanoscale pore and ligament size and their density and distribution, while the external regime refers to shape parameters, such as the disk diameter and thickness. Indeed, we have recently demonstrated long-ranged tuning of NPG nanoparticle plasmonics by varying the disk diameter before de-alloying.<sup>8</sup> In this approach, the plasmon resonance is fixed once the diameter of the NPG nanoparticle is defined. Techniques that can further fine-tune the plasmonic resonance might be of interest due to its *in situ* optimization capability for specific applications.

De-alloying time control and furnace-based thermal annealing are known methods to cause structural alteration as well as plasmonic tuning of the NPG thin films. For example, Lang *et al.* demonstrated pore size tuning from 10 nm to 50 nm by varying the de-alloying time from 5 minutes to 24 hours.<sup>4</sup> This pore size modification shifted the plasmonic peak only by 50 nm. Similarly, Tan and co-workers reported pore size and surface area variations at different temperatures with 0.5 to 3 hours of furnace annealing.<sup>12</sup> Besides higher processing time requirement and limited plasmonic tunability, these techniques have other limitations from the device fabrication standpoint. For example, de-alloying time control may run into material compatibility issues when other materials are involved due to the probable detrimental effects from strong acids employed in de-alloying. Furnace-based thermal annealing, on the other hand, is a slow process and challenging to implement when other materials are onboard with different lower melting points.

<sup>a</sup>Department of Electrical and Computer Engineering, University of Houston, Houston, TX 77204, USA

<sup>b</sup>Department of Biomedical Engineering, University of Houston, Houston, TX 77204, USA. E-mail: wshih@uh.edu

†Electronic supplementary information (ESI) available. See DOI: 10.1039/c4nr03672g

In this paper, we report a novel laser rapid thermal annealing (LRTA) technique for fine-tuning the plasmonic properties of NPG nanoparticles. Unlike in traditional RTA applications where residual stress release is often the primary objective, our LRTA technique aims to cause structural alteration of NPG nanoparticles in as short as 2 minutes. The structural modification causes tuning of plasmonic resonance, which subsequently optimizes the surface-enhanced Raman scattering (SERS) performance *via* better alignment of the excitation laser and Raman scattering wavelengths with the localized surface plasmon resonance (LSPR) peak.

## Methods

Disk-shaped NPG nanoparticles were fabricated utilizing the combination of top-down lithographic patterning and bottom-up atomic de-alloying, thereby suggesting a directed self-assembly technique. An Ag<sub>70</sub>Au<sub>30</sub> (atomic percentage) alloy film with ~50 nm thickness was first sputter deposited on a glass coverslip (~165 μm thick). Then a monolayer of 460 nm diameter polystyrene (PS) beads was formed on top of the alloy film. Next, shrinkage of the PS beads, in order to guarantee the separation between neighboring beads, was done using a timed oxygen plasma treatment. The sample was then sputter etched in argon plasma to transfer the bead pattern into the alloy film. After pattern transfer, PS beads were removed by sonication in chloroform. The remaining alloy disks were then de-alloyed in 70% nitric acid for 1 minute, followed by a 2 minute rinse in de-ionized (DI) water. The de-alloying process resulted in disk-shaped NPG nanoparticles with 300 nm diameter and 46 nm thickness. Further details of the fabrication process can be found elsewhere.<sup>8</sup>

The as prepared NPG nanoparticles were annealed using a 785 nm continuous wave (CW) titanium:sapphire (Spectra-Physics 3900S) laser. Different laser intensities (125, 190, and 250 mW mm<sup>-2</sup>) were used for 120 seconds of exposure. Laser annealing was applied to the nanoparticles on the original glass substrate in air. Time-resolved temperature maps were recorded using an infrared (IR) thermal camera (FLIR A320) from the backside of the glass substrate with no NPG nanoparticles. Thus the temperature measurements were unaffected by any possible emissivity changes during LRTA. Two samples were prepared under the same exposure conditions. One sample was used for extinction and SERS measurements and the other was used for scanning electron microscopy (SEM) (FEI XL-30 FEG SEM, Philips) examination. To obtain SEM images, NPG nanoparticles were sonicated off the substrate in DI water and then dropped on a silicon (Si) substrate. Changes in the pore and disk size were analyzed by visual inspection of the SEM images with the help of the Nano-Measurer 1.2 software. The extinction measurement was performed utilizing a Cary 50 Scan UV-visible spectrometer to characterize the plasmonic properties. After extinction measurements, the sample was incubated in 5 mM benzenethiol (BT) solution for 30 minutes followed by a 1 minute rinse in ethanol to dissolve

unbound BT molecules. Then a line-scan Raman system<sup>13</sup> with a 785 nm continuous wave (CW) laser (Spectra-Physics 3900S) and a 60× water immersion objective lens was used for SERS measurements. Together with low laser intensity and water bath, no temperature rise was observed during the SERS measurements, guaranteeing no further annealing of NPG nanoparticles.

## Results and discussion

### LRTA effects on NPG nanoparticles' morphology

Time resolved temperature maps, associated with different laser power densities, are presented in Fig. 1. The substrate's average temperature was at ~112, 125, and 137 °C with 125, 190, and 250 mW mm<sup>-2</sup> laser intensity, respectively.

The temperature rise induced thermal annealing of NPG nanoparticles, which altered its internal (pore size) and external (disk diameter) morphological features. Fig. 2 shows the SEM images of NPG nanoparticles before and after LRTA. With increasing laser intensity, the average pore size was found to increase, while the mean disk diameter decreased, as shown in Fig. 3(a) and (b) respectively. Table 1 summarizes the numerical results on the pore size and disk diameter for 50 NPG nanoparticles with the corresponding standard deviations.

Furnace-based thermal annealing of semi-infinite NPG thin films has been reported in the literature with results suggesting that the pore size increases with increasing anneal-

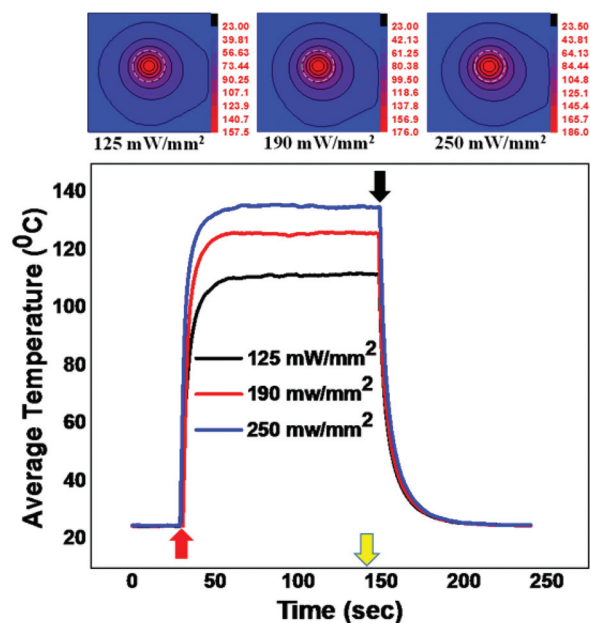


Fig. 1 Average temperature rise for different laser intensities. Red and black arrows indicate laser turning on and off respectively. Contour maps atop represent temperature distributions on ~1 cm × 1 cm coverslip glass with NPG nanoparticles. Dotted circles represent the incident laser beam diameter (3 mm). Yellow arrow indicates the time when contour maps were plotted.

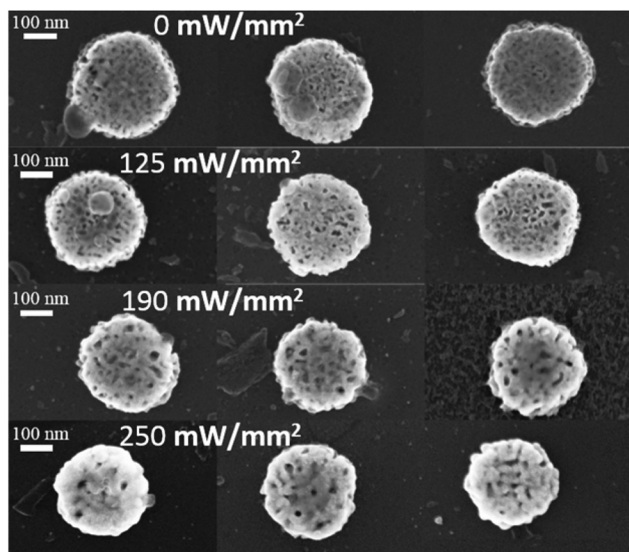


Fig. 2 Disk-shaped NPG nanoparticle morphology before and after LRTA. Each row represents an LRTA condition.

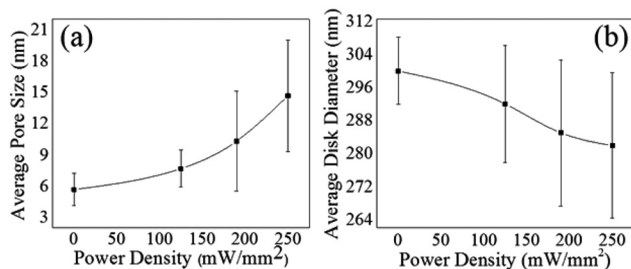


Fig. 3 LRTA induced morphological variations: (a) pore size, (b) disk diameter.

Table 1 Mean and standard deviations of morphological parameters before and after LRTA

Power density (mW mm <sup>-2</sup> )	Pore size (nm)	Disk diameter (nm)
0	5.69 ± 1.54	300 ± 8.14
125	7.7 ± 1.77	292 ± 14.14
190	10.33 ± 4.8	285 ± 17.74
250	14.68 ± 5.34	281 ± 17.64

ing temperature.<sup>12,14</sup> For example, Balk *et al.* reported the increment in pore size from 12 nm to 14 and 30 nm upon annealing with 100 and 200 °C, respectively.<sup>15</sup> The underlying mechanism of this thermal coarsening is the increase in surface diffusion of gold atoms leading to ligament growth and thereby increasing the average pore size.<sup>7</sup> Since a NPG nanoparticle is a special form of a NPG thin film, the pore size increase is also observed for this nanoparticle with thermal annealing. We note that although the pore size increased with increasing laser intensity, the ligament also grew with a seemingly reduction of total pore counts, which could lead to an overall reduction in porosity, as reported for NPG films.<sup>15</sup>

However, LRTA-induced morphological evolution of NPG nanoparticles appears to be significantly different from thermal annealing results in semi-infinite NPG thin films, where pores and ligaments continued to grow at a higher annealing temperature (up to 300 °C). In contrast, the enlarged pores and ligaments coalesce and disappear at much lower temperature (below 200 °C) for NPG nanoparticles. Thus, the differences in morphological evolution between NPG films and NPG nanoparticles should primarily originate from their architecturally distinct features. Heuristically, individual NPG nanoparticles lack the in-plane network organization as seen in the semi-infinite NPG films, leading to a free-to-deform boundary condition around the disk circumference, thereby introducing a prominent annealing effect at even lower temperatures.

It has been reported that thermal annealing of gold nanoparticles causes surface melting which leads to the external size shrinkage.<sup>16</sup> For most nanomaterials, the surface melting point is smaller than their bulk counterparts.<sup>17–19</sup> For example, Wang *et al.* reported platinum (Pt) nanocrystals exhibiting surface melting at ~500 °C, which is much lower than the melting point of bulk Pt (1769 °C).<sup>18</sup> Ong *et al.* reported surface melting and reshaping of non-porous gold nanoparticles at 325 °C.<sup>16</sup> To our knowledge, this is the lowest reported temperature to cause surface melting of gold nanoparticles with comparable (to NPG nanoparticles) dimensions, and is also much smaller than the bulk gold melting temperature (1063 °C). For NPG nanoparticles, however, LRTA causes surface melting and resizing of NPG nanoparticles at temperatures lower than 200 °C. Recently we have reported very high photothermal conversion efficiency (56%) for NPG nanoparticles.<sup>8</sup> This high conversion efficiency along with the porous network is likely to synergistically lower the required annealing temperature.

### LRTA effects on NPG nanoparticles' plasmonics

300 nm NPG nanoparticles exhibit a LSPR peak near 1000 nm. Fig. 4 displays experimentally measured normalized extinction spectra before and after LRTA. Absolute extinction spectra are presented in Fig. S1 of the ESI.† As elucidated in our recent work, NPG nanoparticles exhibit a dominant disk-shape dependent in-plane dipole resonance mode along with an oftentimes degenerated LSPR due to the nanoscale Au ligaments.<sup>8</sup> According to this interpretation, for an unannealed disk, the peak around 1000 nm is the in-plane resonance, and the peak around 600 nm is the NPG LSPR, which is not always obvious because of a significant overlap with the in-plane resonance peak. Below, all our discussion is based on the in-plane resonance mode.

Upon LRTA, we observed blueshifting of the LSPR peak with increasing laser power density. It is well known that for gold nanodisks, the LSPR peak undergoes a blueshift with decreasing diameter due to the changes in electromagnetic retardation.<sup>20,21</sup> However, the degree of blueshift with respect to the diameter to thickness ratio (DTR) ( $\Delta\lambda_{\max}/\Delta\text{DTR}$ ) is about 40 for gold nanodisks,<sup>20</sup> which is much smaller compared to our result ( $\Delta\lambda_{\max}/\Delta\text{DTR} \sim 131$ ). Thus the LRTA-

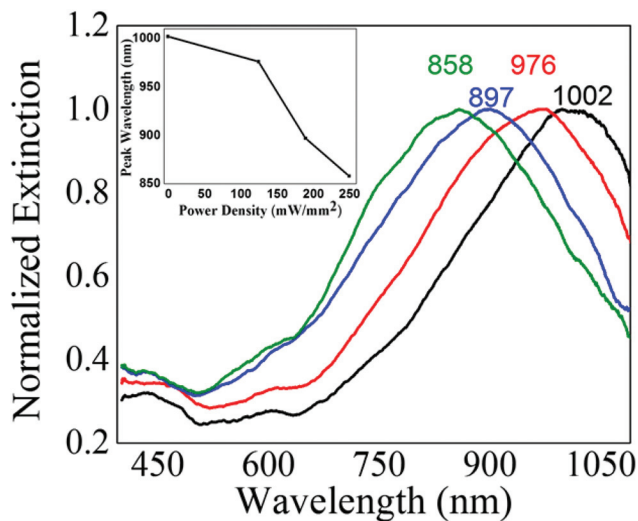


Fig. 4 Normalized extinction spectra of NPG nanoparticles before and after LRTA. The inset represents the peak position.

induced blueshift involves not only the external disk diameter, but also the internal morphological changes.

#### LRTA effects on NPG nanoparticles' SERS performance

Based on Raman scattering, SERS is a sensitive spectroscopic technique for detecting molecular adsorbates on metal nanostructures.<sup>9,22</sup> There has been great interest in the optimization of SERS by maximizing the enhancement factor.<sup>23,24</sup> There are two primary theories for understanding the mechanism of the enhancement effect in SERS. One is electromagnetic theory based on LSPR and the other is chemical theory which posits the formation of charge transfer complexes.<sup>25–27</sup> According to the electromagnetic theory, SERS occurs due to the local electromagnetic field enhancement near the metal structure as a result of the excitation of LSPR. Under this theory, surface enhanced Raman gain<sup>28–32</sup> can be written as

$$G_{\text{SERS}} \propto \left\| \frac{E_{\text{loc}}(\lambda_{\text{exc}}) E_{\text{loc}}(\lambda_{\text{RS}})}{E_0(\lambda_{\text{exc}}) E_0(\lambda_{\text{RS}})} \right\|^2 = g(\lambda_{\text{exc}}) g(\lambda_{\text{RS}}). \quad (1)$$

In eqn (1),  $E_{\text{loc}}(\lambda_{\text{RS}})$  and  $E_0(\lambda_{\text{RS}})$  are the local and incident electric field amplitudes at the Raman wavelength  $\lambda_{\text{RS}}$ , respectively.  $E_{\text{loc}}(\lambda_{\text{exc}})$  and  $E_0(\lambda_{\text{exc}})$  are the local and incident electric field amplitudes at the laser excitation wavelength  $\lambda_{\text{exc}}$ , respectively. According to this equation, the maximum SERS intensity is expected when both the excitation laser wavelength and the Raman wavelength approach the nanostructure's LSPR. Weitz and co-workers have evaluated the SERS intensity as<sup>30,31</sup>

$$I_{\text{SERS}} \propto \frac{1}{4\pi^2 q^2 d^2} \frac{|\epsilon(\lambda_{\text{exc}})|^2 A(\lambda_{\text{exc}}) |\epsilon(\lambda_{\text{RS}})|^2 A(\lambda_{\text{RS}}) \lambda_{\text{exc}} \lambda_{\text{RS}}}{\epsilon_2(\lambda_{\text{exc}}) \epsilon_2(\lambda_{\text{RS}})} \quad (2)$$

In eqn (2),  $A(\lambda) = \left( \frac{2\pi q d \epsilon_2}{\lambda} \right) \left\| \frac{E_{\text{loc}}}{E_0} \right\|^2$  is the local external field-intensity enhancement, where  $d$  and  $q$  represent the film thickness and volume fraction of gold in the film respectively.

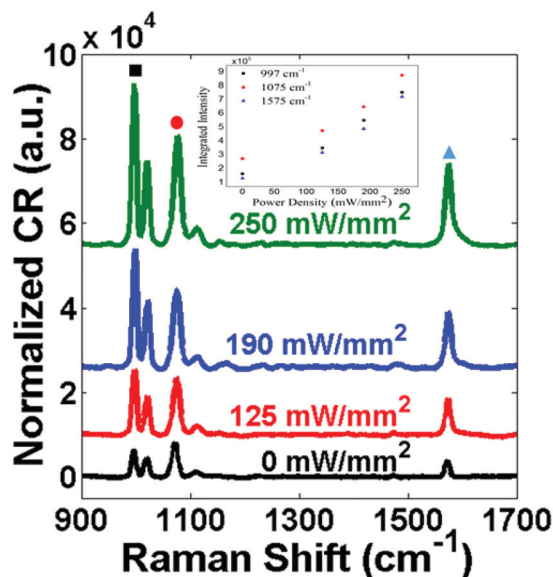


Fig. 5 Normalized count rates (CRs) from BT SAM on NPG nanoparticles under different annealing conditions. The inset represents the integrated intensities for 997, 1075, and 1575  $\text{cm}^{-1}$  Raman bands.

This equation predicts that the maximum SERS intensity should be obtained when the LSPR peak wavelength is equal to the average of the excitation laser and Raman wavelengths, *i.e.*  $\lambda_{\text{max}} = (\lambda_{\text{exc}} + \lambda_{\text{RS}})/2$ ,<sup>33</sup> which has been experimentally verified in several publications.<sup>34,35,37</sup>

By tuning the plasmonic resonance, our LRTA technique can potentially provide a rapid and non-invasive way to fine-tune the SERS performance of NPG nanoparticles. Fig. 5 shows the SERS spectra, presented in the CCD count rate (CR), normalized to the laser power and spot area, of the benzethiol (BT) self-assembled monolayer (SAM) on NPG nanoparticles before and after LRTA.

From Fig. 5, it is noted that the 1575  $\text{cm}^{-1}$  Raman band intensity increases with increasing laser power density. In our experiment we used a 785 nm laser and the Stokes Raman scattering wavelength corresponding to the 1575  $\text{cm}^{-1}$  band is at 895 nm. Thus the maximum SERS intensity should be obtained when the LSPR peak wavelength approaches  $((785 + 895)/2) \sim 840$  nm. As seen in Fig. 4, with increasing laser power density the LSPR peak blue shifted towards 840 nm, thereby enhancing the SERS intensity. Similar explanations also stand for the enhancement of other Raman band intensities. The inset of Fig. 5 represents the enhancement in integrated intensities for different Raman bands with LRTA. Zeng *et al.* studied the structural alterations of NPG nanoparticles under different post fabrication furnace annealing conditions and reported SERS intensity decrement with increasing annealing temperature.<sup>36</sup> As reported there, surface roughness plays an important role in SERS enhancement. With furnace annealing, higher temperature and longer annealing time result in the regrowth of NPG nanoparticles to form smooth surfaces. In contrast, for LRTA, lower annealing temperature

and shorter duration roughen the particle surface more, thereby enhancing the SERS intensity.

The SERS enhancement factor is inversely proportional to the number of SERS contributing molecules that are related to the surface area of NPG nanoparticles. The “apparent” surface area for 250 mW mm<sup>-2</sup> annealed NPG nanoparticles is ~6 times smaller compared to unannealed ones (surface area calculation is provided in ESI†). Thus although the normalized CR for the 1575 cm<sup>-1</sup> Raman band is ~5 times larger for NPG nanoparticles annealed with 250 mW mm<sup>-2</sup> laser intensity, the actual increase of SERS enhancement could be larger than 5 times.

Although we used a 3 mm laser spot, our technique is scalable, *i.e.* the beam diameter can be increased by increasing the total laser power while maintaining similar power density we used in our experiment. However, this technique is even more powerful to alter nanoparticles on the same substrate differently. It is possible to obtain a highly focused micron scale laser spot pattern<sup>38,39</sup> and apply LRTA selectively over selected micron spots with high throughput, which will be our future work.

## Conclusions

In conclusion, we have reported a novel LRTA technique for tuning plasmonic resonance of disk-shaped NPG nanoparticles at much lower temperatures compared to bulk gold and non-porous gold nanoparticles. We have investigated the variations in both internal and external morphological structures under different annealing conditions. With increasing annealing laser intensity, we found an increase in pore size with reducing pore coverage and a decrease in disk diameter. These morphological changes led to blueshifting of the in-plane LSPR resonance peak. The LSPR tuning can be potentially valuable for plasmonic applications of NPG nanoparticles. As an example, we have demonstrated the fine-tuning of SERS enhancement with 785 nm laser excitation.

## Acknowledgements

Wei-Chuan Shih acknowledges the National Science Foundation (NSF) CAREER Award (CBET-1151154), the National Aeronautics and Space Administration (NASA) Early Career Faculty Grant (NNX12AQ44G) and a grant from the Gulf of Mexico Research Initiative (GoMRI-030).

## References

- C. Xu, J. Su, X. Xu, P. Liu, H. Zhao, F. Tian and Y. Ding, *J. Am. Chem. Soc.*, 2006, **129**, 42–43.
- A. Wittstock, J. Biener and M. Baumer, *Phys. Chem. Chem. Phys.*, 2010, **12**, 12919–12930.
- D. Kramer, R. N. Viswanath and J. Weissmüller, *Nano Lett.*, 2004, **4**, 793–796.
- X. Lang, L. Qian, P. Guan, J. Zi and M. Chen, *Appl. Phys. Lett.*, 2011, **98**, 093701–093703.
- F. Meng and Y. Ding, *Adv. Mater.*, 2011, **23**, 4098–4102.
- F. Jia, C. Yu, Z. Ai and L. Zhang, *Chem. Mater.*, 2007, **19**, 3648–3653.
- E. Seker, M. Reed and M. Begley, *Materials*, 2009, **2**, 2188–2215.
- F. Zhao, J. Zeng, M. M. P. Arnob, P. Sun, J. Qi, J. C. Wolfe, P. Motwani, M. Gheewala, T. R. Lee, C.-H. Li, R. Willson, U. Strych, A. Paterson, B. Raja and W.-C. Shih, *Nanoscale*, 2014, **6**, 8199–8207.
- J. Qi, P. Motwani, M. Gheewala, C. Brennan, J. C. Wolfe and W.-C. Shih, *Nanoscale*, 2013, **5**, 4105–4109.
- M. Li, J. Lu, J. Qi, F. Zhao, J. Zeng, J. C.-C. Yu and W.-C. Shih, *J. Biomed. Opt.*, 2014, **19**, 050501–050501.
- G. M. Santos, F. Zhao, J. Zeng and W.-C. Shih, *Nanoscale*, 2014, **6**, 5718–5724.
- Y. H. Tan, J. A. Davis, K. Fujikawa, N. V. Ganesh, A. V. Demchenko and K. J. Stine, *J. Mater. Chem.*, 2012, **22**, 6733–6745.
- J. Qi and W.-C. Shih, *Appl. Opt.*, 2014, **53**, 2881–2885.
- E. Seker, J. T. Gaskins, H. Bart-Smith, J. Zhu, M. L. Reed, G. Zangari, R. Kelly and M. R. Begley, *Acta Mater.*, 2007, **55**, 4593–4602.
- Y. Sun, K. P. Kucera, S. A. Burger and T. John Balk, *Scr. Mater.*, 2008, **58**, 1018–1021.
- B. J. Y. Tan, C. H. Sow, T. S. Koh, K. C. Chin, A. T. S. Wee and C. K. Ong, *J. Phys. Chem. B*, 2005, **109**, 11100–11109.
- K. K. Nanda, S. N. Sahu and S. N. Behera, *Phys. Rev. A*, 2002, **66**, 013208.
- Z. L. Wang, J. M. Petroski, T. C. Green and M. A. El-Sayed, *J. Phys. Chem. B*, 1998, **102**, 6145–6151.
- J. C. Hulteen, D. A. Treichel, M. T. Smith, M. L. Duval, T. R. Jensen and R. P. Van Duyne, *J. Phys. Chem. B*, 1999, **103**, 3854–3863.
- I. Zorić, M. Zäch, B. Kasemo and C. Langhammer, *ACS Nano*, 2011, **5**, 2535–2546.
- P. Hanarp, M. Käll and D. S. Sutherland, *J. Phys. Chem. B*, 2003, **107**, 5768–5772.
- W.-C. Shih, K. Bechtel and M. S. Feld, *Analytical chemistry of in vivo glucose measurements*, John Wiley & Sons, Hoboken, NJ, 2009, ch. 14, pp. 391–419.
- J. Qi, J. Zeng, F. Zhao, S. H. Lin, B. Raja, U. Strych, R. C. Willson and W.-C. Shih, *Nanoscale*, 2014, **6**, 8521–8526.
- M. Li, F. Zhao, J. Zeng, J. Qi, J. Lu and W.-C. Shih, *J. Biomed. Opt.*, 2014, **19**, 111611.
- M. Moskovits, *Rev. Mod. Phys.*, 1985, **57**, 783–826.
- A. Otto, *J. Raman Spectrosc.*, 1991, **22**, 743–752.
- F. R. Aussenegg and M. E. Lippitsch, *Chem. Phys. Lett.*, 1978, **59**, 214–216.
- M. Kerker, D. S. Wang and H. Chew, *Appl. Opt.*, 1980, **19**, 3373–3388.

- 29 P. K. Aravind, A. Nitzan and H. Metiu, *Surf. Sci.*, 1981, **110**, 189–204.
- 30 D. A. Weitz, S. Garoff and T. J. Gramila, *Opt. Lett.*, 1982, **7**, 168–170.
- 31 D. A. Weitz, S. Garoff, J. I. Gersten and A. Nitzan, *J. Chem. Phys.*, 1983, **78**, 5324–5338.
- 32 H. G. Bingler, H. Brunner, A. Leitner, F. R. Aussenegg and A. Wokaun, *Mol. Phys.*, 1995, **85**, 587–606.
- 33 N. Féridj, J. Aubard, G. Lévi, J. R. Krenn, M. Salerno, G. Schider, B. Lamprecht, A. Leitner and F. R. Aussenegg, *Phys. Rev. B: Condens. Matter*, 2002, **65**, 075419.
- 34 J. Grand, M. L. de la Chapelle, J. L. Bijeon, P. M. Adam, A. Vial and P. Royer, *Phys. Rev. B: Condens. Matter*, 2005, **72**, 033407.
- 35 C. L. Haynes and R. P. Van Duyne, *J. Phys. Chem. B*, 2003, **107**, 7426–7433.
- 36 J. Zeng, F. Zhao, J. Qi, Y. Li, C.-H. Li, Y. Yao, T. R. Lee and W.-C. Shih, *RSC Adv.*, 2014, **4**, 36682–36688.
- 37 A. D. McFarland, M. A. Young, J. A. Dieringer and R. P. Van Duyne, *J. Phys. Chem. B*, 2005, **109**, 11279–11285.
- 38 J. Qi and W.-C. Shih, *Opt. Lett.*, 2012, **37**, 1289–1291.
- 39 J. Qi, J. Li and W.-C. Shih, *Biomed. Opt. Express*, 2013, **4**, 2376–2382.